Supplemental Material for:

Solid-solid phase transitions across orientationally disordered phases: the case of tetrachlorometaxylene

Jonathan F. Gebbia[1,2,*], Ares Sanuy[1,2], Michela Romanini[1,2], David Aguilà[3], Phillipe Negrier[4], Stephane Negrier[5], María del Barrio[1,2], Felix Fernandez-Alonso[6,7,8], Sanghamitra Mukhopadhyay[9], Markus Apple[10], Claudio Cazorla[1,2,11], Luis Carlos Pardo[1,2], Josep Ll. Tamarit[1,2].

[1]Grup de Caracterització de Materials, Departament de Física, EEBE, Universitat Politècnica de Catalunya, Eduard Maristany, 10-14, 08019 Barcelona, Catalonia, Spain

[2]Barcelona Research Center in Multiscale Science and Engineering, EEBE, Universitat Politècnica de Catalunya, Eduard Maristany, 10-14, 08019 Barcelona, Catalonia, Spain

[3]Departament de Química Inorgànica, and Institute of Nanoscience and Nanotechnology (IN2UB), Universitat de Barcelona, Barcelona, Spain

[4]Laboratoire Ondes et Matière d'Aquitaine, Université de Bordeaux, UMR 5798, F-33400 Talence, France

[5]Institut Europeen Chimie & Biologie, Universite de Bordeaux, CNRS UMS 3033, INSERM US001, F-33607 Pessac, France

[6]Centro de Física de Materiales (CFM-MPC), CSIC-UPV/EHU, Paseo de Manuel Lardizabal 5, Donostia, 20018, Gipuzkoa, Spain

[7]Donostia International Physics Center (DIPC), Paseo de Manuel Lardizabal 4, 20018 Donostia - San Sebastian, Spain

[8]IKERBASQUE, Basque Foundation for Science, Plaza Euskadi 5, 48009 Bilbao, Spain

[9]ISIS Neutron and Muon Source, Rutherford Appleton Laboratory, Chilton, Didcot, Oxfordshire OX11 0QX, United Kingdom

[10]Institut Laue-Langevin (ILL), 71 Av. Des Martyrs, 38000 Grenoble, France

[11]Institució Catalana de Recerca i Estudis Avançats (ICREA), Passeig Lluís Companys 23, 08010 Barcelona, Spain

[*] Corresponding author. jonathan.fernando.gebbia@upc.edu

I. X-Ray diffraction

Table S1. Crystal data and structure refinement for low-temperature phase II of TCMX from single crystal diffraction.

Identification code	TCMX	
Empirical formula	$C_8H_6Cl_4$	
Formula weight	243.93	
Temperature	100(2) K	
Wavelength	0.71073 Å	
Crystal system	Monoclinic	
Space group	$P2_1/n$	
Unit cell dimensions	$a = 8.0537(6)$ Å	$\alpha = 90°$
	$b = 3.7958(2)$ Å	$\beta = 92.038(5)°$
	$c = 14.8015(9)$ Å	$\gamma = 90°$

Volume	452.20(5) Å^3
Z	2
Density (calculated)	1.791 Mg/m^3
Absorption coefficient	1.242 mm^{-1}
F(000)	244
Crystal size	0.270 × 0.060 × 0.060 mm^3
Theta range for data collection	2.838 to 27.475°.
Index ranges	$-8 \leq h \leq 10, -4 \leq k \leq 4, -17 \leq l \leq 19$
Reflections collected	4074
Independent reflections	1036 [R(int) = 0.0266]
Completeness to theta = 25.242°	99.6 %
Absorption correction	Semi-empirical from equivalents
Max. and min. transmission	0.925 and 0.912
Refinement method	Full-matrix least-squares on F^2
Data / restraints / parameters	1036 / 3 / 73
Goodness-of-fit on F^2	1.007
Final R indices [$I > 2\sigma(I)$]	$R1 = 0.0295, wR2 = 0.0730$
R indices (all data)	$R1 = 0.0350, wR2 = 0.0763$
Extinction coefficient	n/a
Largest diff. peak and hole	0.297 and −0.278 e.Å^{-3}
CCDC number	2490401

Table S2. Results from the Rietveld refinement of phases II and I from powder X-ray diffraction measurements for phases II (at 100 K) and I (at 460 K).

Parameter	**Phase II (100 K)**	**Phase I (460 K)**
2θ-Angular Range (°)	10-80	10-50
2θ-shift (zero correction)	0.0362(11)	0.005(6)
Crystal system	Monoclinic	Orthorhombic
Space group	$P2_1/n$	$Pnnm$
Z / Z'	2 / 0.5	2 / 0.25
Profile Parameters		
Na	0.397(13)	0.25(4)
Nb	0	0
Lattice parameters		
a /Å	8.0565(9)	15.250(7)

b / Å	3.7959(5)	3.9539(9)
c / Å	14.8044(16)	8.4235(25)
α / °	90	90
β / °	91.945(2)	90
γ / °	90	90
Reliability Parameters		
${}^{*}R_{wp}$	4.77	3.36
${}^{**}R_{p}$	3.52	2.51
Peak width parameters		
u	0.377(16)	0.20(12)
v	-0.217(10	-0.17(5)
w	0.0536(17)	0.044(6)
Overall isotropic temperature factor, U / Å^2	0.0098(5)	0.313(18)
Preferred Orientation (March Dollase function)		
a^*	0.097(24)	0.668(10)
b^*	0.4584(18)	0.439(6)
c^*	0.883(11)	0.601(9)
R_0	1.143(5)	0.256(14)

${}^{*}R_{wp} = \frac{\sum_i w_i |cY^{sim}(2\theta_i) - I^{exp}(2\theta_i) + Y^{back}(2\theta_i)|^2}{\sum_i w_i |I^{exp}(2\theta_i)|^2}$, ${}^{**}R_p = \frac{\sum_i |cY^{sim}(2\theta_i) - I^{exp}(2\theta_i) + Y^{back}(2\theta_i)|^2}{\sum_i |I^{exp}(2\theta_i)|^2}$

Table S3. Lattice parameters as a function of temperature for phase II (monoclinic $P2_1/n$, $Z = 2$) and phase I (orthorhombic $Pnnm$, $Z = 2$)

Phase	***T*/K**	***a*/Å**	***b*/Å**	***c*/Å**	***β*/º**	***V*/*Z* Å^3/molec**
II	100	8,0575(2)	3,7964(1)	14,8061(5)	91,942(1)	226,32(1)
	110	8,0614(4)	3,7999(2)	14,8151(8)	91,915(2)	226,78(2)
	120	8,0648(4)	3,8031(3)	14,8231(9)	91,886(3)	227,19(2)
	130	8,0676(4)	3,8061(2)	14,8319(8)	91,864(2)	227,59(2)
	140	8,073(3)	3,8102(2)	14,8431(8)	91,829(2)	228,16(2)
	150	8,0784(4)	3,8135(3)	14,8529(8)	91,807(3)	228,67(2)
	160	8,0831(4)	3,8171(2)	14,8623(8)	91,785(3)	229,17(2)
	170	8,088(4)	3,8207(2)	14,8726(8)	91,749(3)	229,68(2)
	200	8,1025(4)	3,8328(2)	14,8999(9)	91,661(3)	231,26(2)
	230	8,1221(4)	3,8467(2)	14,9291(9)	91,589(3)	233,12(2)
	260	8,1355(4)	3,8575(3)	14,9519(10)	91,507(3)	234,53(2)
	290	8,1559(5)	3,8719(3)	14,9805(14)	91,428(3)	236,46(3)
	300	8,1628(5)	3,8782(3)	14,9964(10)	91,456(3)	237,29(2)
	320	8,1778(5)	3,885(3)	15,0087(12)	91,347(3)	238,35(3)
	350	8,2061(6)	3,901(3)	15,0429(13)	91,273(3)	240,72(3)
	377,9	8,2425(5)	3,9179(3)	15,0819(12)	91,201(3)	243,46(3)
	396,4	8,2662(4)	3,9338(2)	15,1276(8)	91,102(3)	245,66(2)
	405,7	8,285(5)	3,9328(2)	15,1207(10)	91,067(3)	246,29(3)
	419,6	8,2622(14)	3,9440(6)	15,1410(24)	90,946(12)	246,66(6)
	428,8	8,3305(10)	3,9505(6)	15,1890(18)	90,949(5)	249,89(3)
	433,5	8,3482(9)	3,9489(4)	15,1829(15)	90,866(7)	250,23(4)
	438,1	8,3538(18)	3,9480(7)	15,1751(20)	90,794(11)	250,22(2)
	440,4	8,3975(5)	3,9501(2)	15,2042(8)	90,269(3)	252,16(2)
	442,7	8,3944(8)	3,9496(4)	15,1939(17)	90,347(7)	251,87(4)
						226,32(1)
I	447,4	15,2559(2)	3,9539(6)	8,4123(1)		253,71(5)
	452	15,2531(12)	3,9568(4)	8,4293(8)		254,37(3)
	461,3	15,2564(12)	3,9602(3)	8,4364(7)		254,86(3)
	470,5	15,2392(11)	3,9614(3)	8,4369(6)		254,64(7)

Table S4. Fractional atomic coordinates and occupancies for TCMX in the low-temperature phase II at 100 K.

Atom	x	y	z	Occupancy
C1	0.6227(2)	0.6336(5)	0.55931(12)	1
C2	0.6522(2)	0.6086(5)	0.46749(12)	1
C3	0.5296(2)	0.4738(5)	0.40797(12)	1
Cl1	0.7749(2)	0.7951(7)	0.63284(14)	0.6667
Cl2	0.8394(2)	0.7466(7)	0.42752(16)	0.6667
Cl3	0.5670(3)	0.4419(7)	0.29488(9)	0.6667
C4	0.750(2)	0.775(5)	0.6275(11)	0.3333
H4A	0.6946	0.9243	0.6713	0.3333
H4B	0.8329	0.9137	0.5963	0.3333
H4C	0.8048	0.5777	0.6593	0.3333
C5	0.8141(15)	0.725(6)	0.4286(14)	0.3333
H5A	0.7944	0.9303	0.3895	0.3333
H5B	0.8599	0.5323	0.3930	0.3333
H5C	0.8931	0.7874	0.4779	0.3333
C6	0.564(2)	0.444(5)	0.3086(4)	0.3333
H6A	0.6754	0.3437	0.3016	0.3333
H6B	0.5590	0.6778	0.2808	0.3333
H6C	0.4813	0.2897	0.2790	0.3333

Table S5 Anisotropic displacement parameters U_{ij} ($Å^2$) for the non-hydrogen atoms of TCMX in the low-temperature phase II at 100 K. The labeling scheme of the atoms corresponds to that used in the deposited CIF file.

Atom	U11	U22	U33	U23	U13	U12
C1	0.0167(8)	0.0140(9)	0.0205(9)	0.0003(7)	-0.0031(6)	0.0026(7)
C2	0.0141(8)	0.0149(9)	0.0207(9)	0.0025(7)	0.0005(6)	0.0017(7)
C3	0.0190(8)	0.0148(9)	0.0163(8)	-0.0002(7)	0.0005(6)	0.0029(7)
Cl1	0.0168(7)	0.0241(6)	0.0239(5)	-0.0029(4)	-0.0061(4)	-0.0029(5)
Cl2	0.0132(5)	0.0285(6)	0.0249(5)	0.0035(4)	0.0031(5)	-0.0032(5)
Cl3	0.0263(6)	0.0353(6)	0.0162(4)	-0.0010(5)	0.0017(4)	0.0022(4)
C4	0.009(3)	0.014(3)	0.025(4)	0.002(2)	-0.002(2)	-0.003(2)
C5	0.009(3)	0.014(3)	0.025(4)	0.002(2)	-0.002(2)	-0.003(2)
C6	0.009(3)	0.014(3)	0.025(4)	0.002(2)	-0.002(2)	-0.003(2)

Table S6. Fractional atomic coordinates and occupancies for TCMX in the high-temperature phase I at 460 K.

Atom	x	y	z	Occupancy
C1	0.45548(6)	0.5560(8)	0.35787	0.5000
C2	0.54528(14)	0.6187(8)	0.36748	0.5000
C3	0.58980(7)	0.5627(15)	0.50961	0.5000
Cl1	0.40050(14)	0.6253(17)	0.18231	0.3333
Cl2	0.6012(3)	0.7654(17)	0.20379	0.3333
Cl3	0.70072(16)	0.640(3)	0.52148	0.3333
C4	0.40730(13)	0.6167(16)	0.20402	0.1667
H4A	0.3855(4)	0.8498(19)	0.20147	0.1667
H4B	0.35775(5)	0.460(2)	0.19604	0.1667
H4C	0.44733(9)	0.5800(9)	0.11465	0.1667
C5	0.5943(3)	0.7473(16)	0.22404	0.1667
H5A	0.61626(6)	0.555(2)	0.16222	0.1667
H5B	0.6438(4)	0.887(2)	0.25862	0.1667
H5C	0.5547(4)	0.8828(9)	0.15810	0.1667
C6	0.68700(15)	0.631(3)	0.52001	0.1667
H6A	0.6967(4)	0.865(3)	0.55303	0.1667
H6B	0.71348(3)	0.477(4)	0.59790	0.1667
H6C	0.71398(11)	0.593(4)	0.41589	0.1667

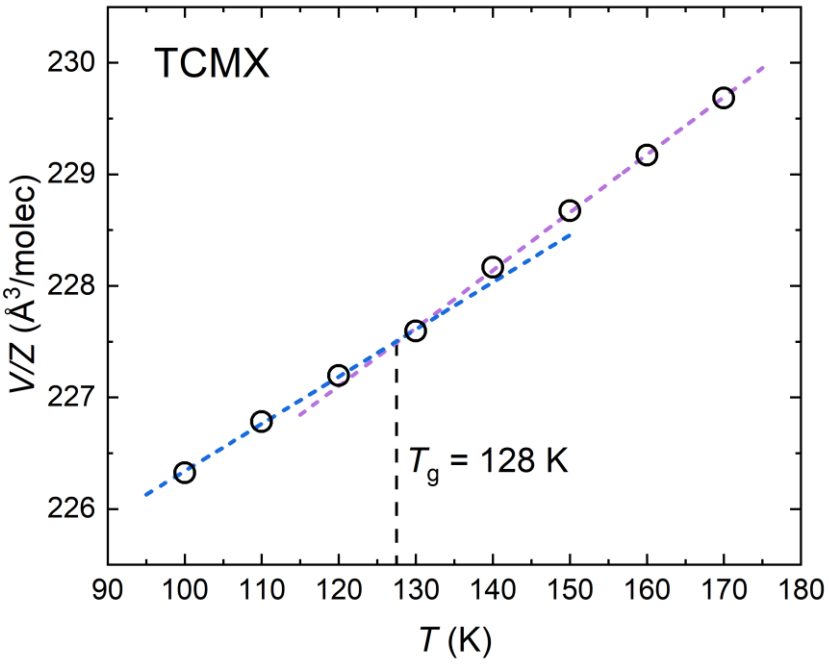

Figure S1. Unit cell volume of TCMX as a function of temperature between 100 and 170 K. Vertical dashed black line indicates the glass transition temperature, where a change in the slope of V/Z is detected.

II. Quasielastic Neutron Scattering – model selection

Fitting QENS spectra requires careful model selection, as the inclusion of additional relaxation processes can improve the fit at the cost of potential overfitting. To ensure a statistically robust model selection, we employed the Bayesian fitting algorithm FABADA, which evaluates the Probability Distribution Function (PDF) of χ^2 for competing models with different numbers of Lorentzian components. Figure S2 shows the comparison of χ^2 distributions for the models tested: (i) one Lorenzian, (ii) one Lorentzian + flat background, and (iii) two Lorentzians.

As shown in Fig. S2, adding a flat background significantly improves the fit compared to a single Lorentzian alone, while the inclusion of a second Lorentzian does not provide meaningful information despite the improvement of the fitting. In fact, the additional component systematically appears with a linewidth larger than the dynamic range of the instrument, yielding *de facto* to a flat background. For this reason, all subsequent analyses were performed using a model consisting of one Lorentzian term plus a flat background.

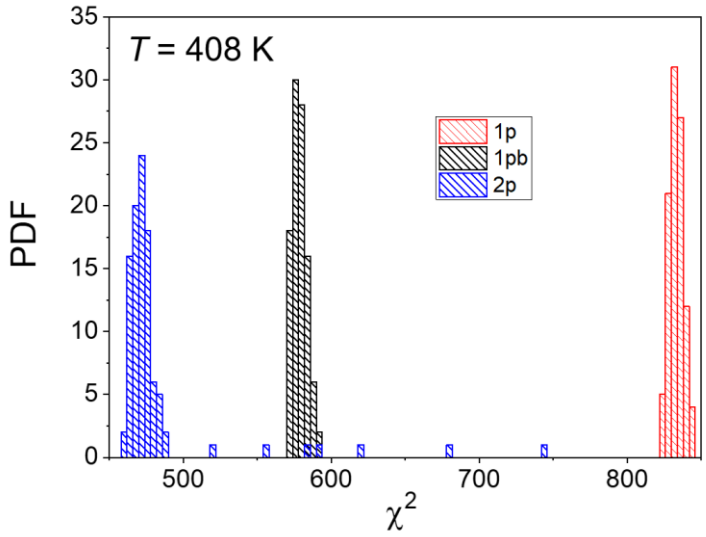

Figure S2. Probability Distribution Function (PDF) of the χ^2 for the models tested using FABADA on a selected spectrum taken at 408 K: (i) one Lorentzian (red), (ii) one Lorentzian plus a flat background (black), and (iii) two Lorentzians (blue).